Plasmonics (2022) 17:2197–2204
https://doi.org/10.1007/s11468-022-01707-7

Simulation and Analysis of Ring Shape Metal–Insulator-Metal Plasmonic Biosensors for the Detection of Prostate-Specific Antigen (PSA)

Younes Majd Shokorlou[1] · Hamid Heidarzadeh[1] · Hamid Bahador[1]

Received: 4 April 2022 / Accepted: 30 August 2022 / Published online: 15 September 2022

Abstract
In this paper, a plasmonic refractive index sensor based on metal–insulator-metal (MIM) topology in the form of a nanoring was investigated for the detection of prostate-specific antigen (PSA), which was validated using the finite-difference time-domain (FDTD) three-dimensional numerical equation method. We have tried to get the most optimal state of the nanoring-shaped sensor using various simulations. Here, two different types of metals (Au and Ag) in two different shapes of ring and disk were examined. The results of this study show the superiority of nanoring-shaped sensors to disk and the relative superiority of Ag to Au. The highest sensitivity and FOM for detecting PSA in the Ag nanoring shape are 567.23 and 3.72 nm/RIU, respectively, while these values are 478.34 and 2.91 nm/RIU for disk shapes, respectively. The wavelength range of the sensor is very close to the information communication window. In addition to its remarkable sensor capability, it can also be used in optical electronics applications such as optical switching, amplifiers, and all-optical plasmon modulators.

Keywords Biosensor · Metal-insulator-metal · Nanoring · Plasmonic · Prostate-specific antigen (PSA)

Introduction

Prostate cancer remains one of the most common cancers worldwide [1] and is usually diagnosed by testing serum levels of prostate-specific antigen (PSA). Despite the great importance and use of PSA, there are inherent limitations due to the limited specificity that lead to a significant rate of unnecessary biopsy [2]. In addition, PSA screening is unsatisfactory, and therefore, there is disagreement about the cancer benefits of prostate cancer screening with PSA. High-volume trials have shown a 20% reduction in prostate cancer mortality in patients undergoing PSA screening [3]. Accordingly, there is a great need to improve methods for assessing prostate cancer risk. The introduction of new imaging modalities, including multimeter MRI (mpMRI), has improved the diagnosis of prostate cancer [4–6]. However, mpMRI is expensive and not widely available, so optimal patient selection is crucial for diagnosis. Various strategies have been added to clinical practice to improve the sensitivity and risk classification of PSA-based prostate cancer. Such strategies include PSA-based kinetics (PSA velocity), utilization of total free PSA ratio, and PSA density (based on prostate volume). Especially those with PSA between 4.0 and 10 ng/ml [7, 8]. To provide specific binding of PSA, there are several methods like the immuno-PCR (IPCR), bio-barcode assay, surface-enhanced Raman scattering (SERS), and electrical detection of micro-cantilever bending [9–12]. IPCR is a technique where after PSA capture by anti-PSA antibodies on the surface of a biosensor, a DNA-labeled detection antibody binds. IPCR is a powerful method for detecting low quantities of protein antigens [9]. Bio-barcode assay is a rapid and ultrasensitive tool for detecting biological targets such as proteins and nucleic acids in the entire sample [10]. In SERS, binding of PSA to anti-PSA antibodies functionalized with Raman reporter molecules (RRMs) and immobilized onto gold microparticles leads to the altered spectroscopic output of the RRMs, which can be used to quantify the concentration of PSA [11]. In the electrical detection of the micro-cantilever bending technique, piezoresistive microcantilevers, functionalized with anti-PSA antibodies, bend owing to surface stress caused by PSA capture. Microcantilever bending is measured by electrical detection [12]. Surface plasmon biosensors are a sensor designed based on

✉ Hamid Heidarzadeh
heidarzadeh@uma.ac.ir

[1] Department of Electrical and Computer Engineering, University of Mohaghegh Ardabili, Ardabil, Iran

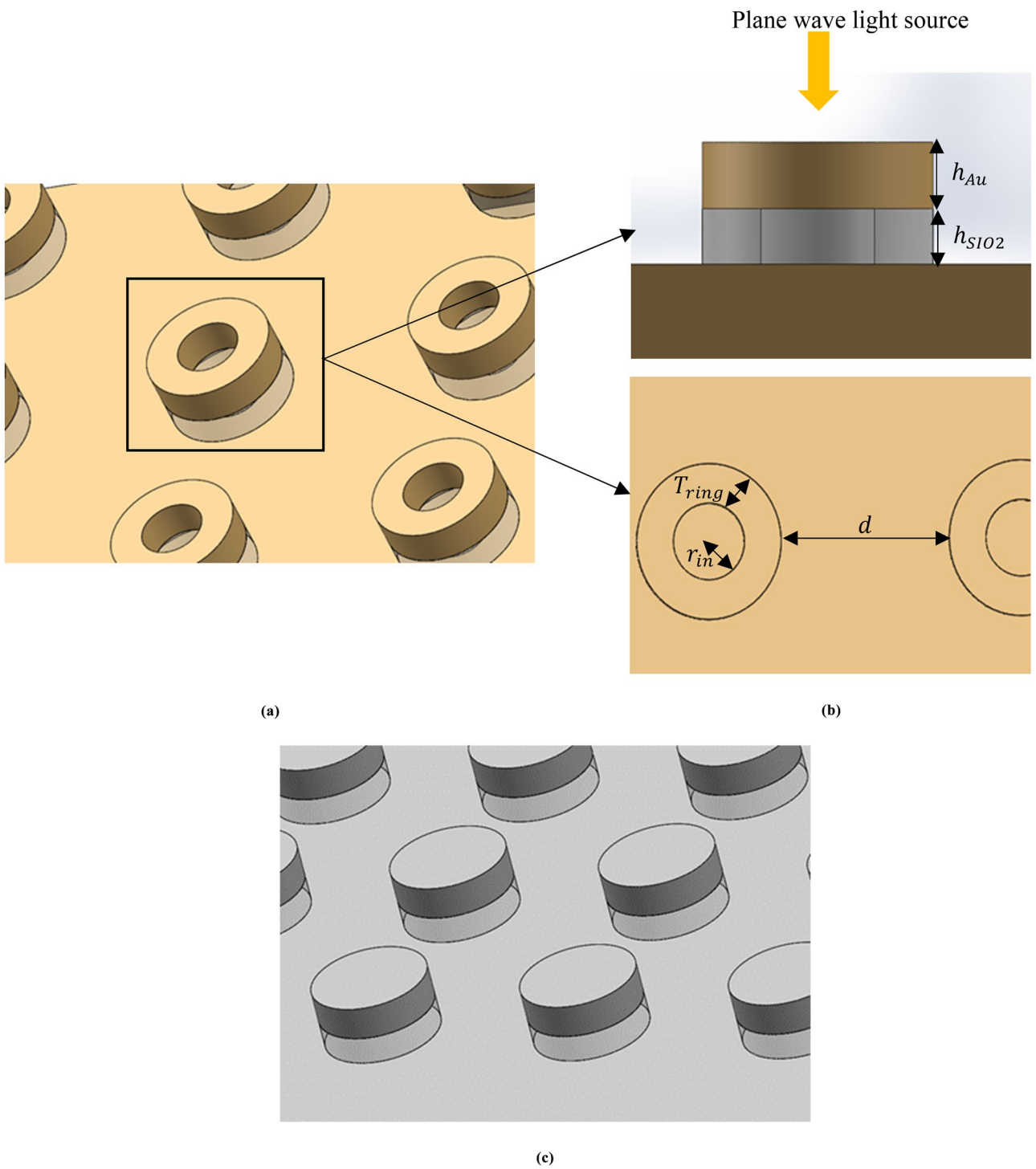

Fig. 1 **a** The proposed ring shape MIM-based biosensor. **b** The different cross-sections views of ring shape biosensor and **c** disk-shaped biosensors

the surface plasmon resonance (SPR) phenomenon to detect biological substances. The basic principle is based on the specific binding of chemical molecules or biomolecules on the material's surface, resulting in the change of the local refractive index of the environment and the change of the surface plasmon resonance frequency. In recent years, rapid and accurate point-of-care medical diagnosis and biological detection have attracted more and more attention, and surface plasmon biosensors have also become a hot topic in scientific research. Its label-free detection method has become one of the unique

Table 1 Refractive index for different concentrations of PSA $(n_0 = 1.33)$

C (pMPSA)	$N = n_0 + \Delta n$
50	1.3388
100	1.3477
200	1.3654
300	1.3831
400	1.4008
500	1.4185

advantages of this type of material. In the surface plasmon polariton (SPP)-type biosensors, electromagnetic waves are emitted at the interface between metal and dielectric materials Many optical components, such as filters [13, 14], sensors [15], and amplifiers [16, 17], have been reported using SPP waves. Among the mentioned applications, refractive index sensors have many applications. They have been widely used in biomedical applications such as cancer diagnosis [18–20], blood component measurements [19–21], and health care programs [22]. Instruments that use surface plasmons are usually much smaller in area than conventional optical components, optical fibers, and photon crystal devices. This feature is an excellent reason to use them as bio-implantable sensors. In addition, it became higher sensitivities using SPPs than other methods such as photon crystals. Despite the different configurations of plasmonic sensors, MIM topologies can be a good choice for efficiently transmitting electrical and optical signals in an integrated circuit. Due to the unique optical properties that MIM configurations show, they have been highly regarded by researchers in the design of optical devices [23]. The MIM topology, due to the severe confinement of the electric field and the long propagation amplitude, maximizes the interaction length of the field with the sensing substance and has received considerable attention [24]. Early detection of cancer makes treatment more effective and cheaper, so by identifying a specific antigen, we can detect cancer earlier than it spreads. In this article, we use prostate-specific antigens for the early detection of prostate cancer. We propose a nanoring-shaped biosensor based on local surface plasmon resonance (LSPR) using the MIM topology. We use FDTD for validation and show that the proposed structure performs better than the disk structure and can be used to detect prostate-specific antigens. Because this is an optical detection method, the sensor is sensitive to changes in surface refractive index.

The Structure Design and Simulation Methodology

In this section, we present the proposed structure and governing equations for PSA detection. Figure 1a shows the proposed structure. As it is evident in this figure, the proposed

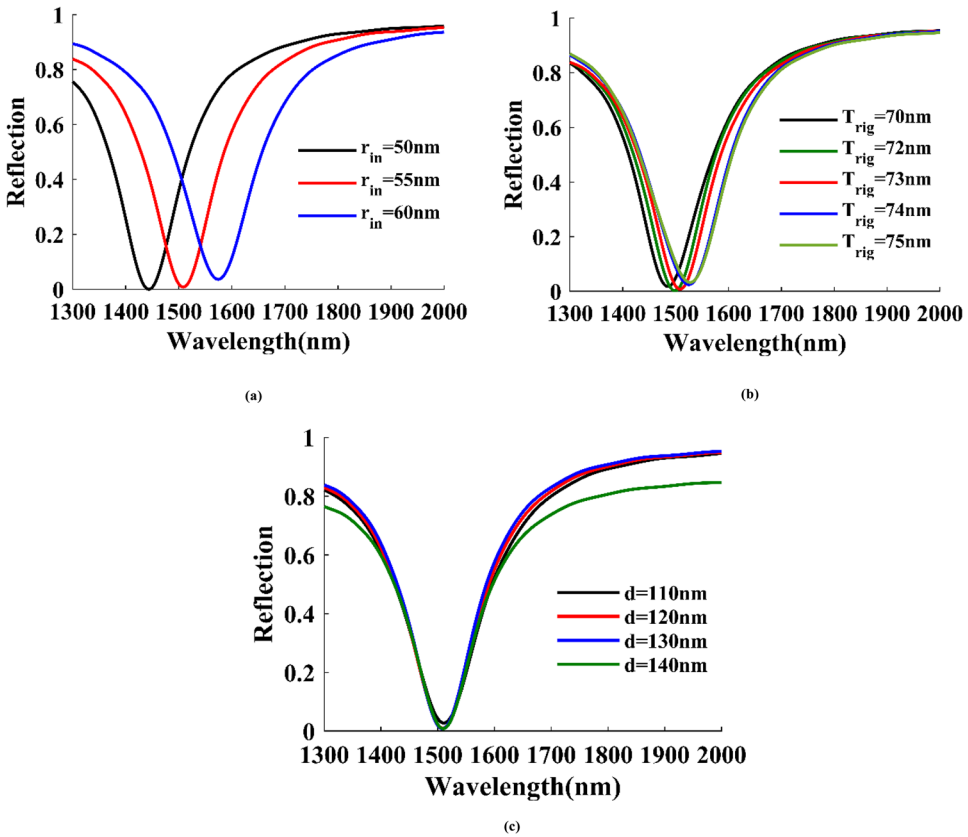

Fig. 2 Reflection of Au ring shape NPs as a function of the wavelength for **a** different inner radii of the ring, **b** different thicknesses of the ring, and **c** different distances of adjacent ring

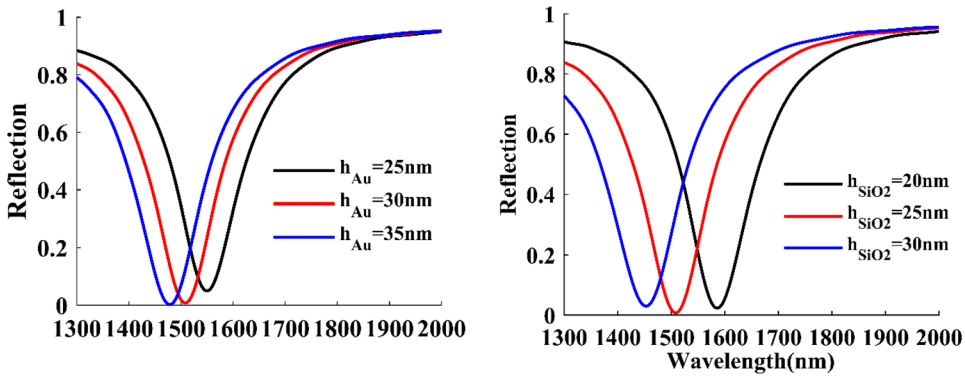

Fig. 3 Reflection of Au ring-shape NPs as a function of the wavelength for **a** effect of Au height and **b** effect of SiO_2 heights

structure consists of a base layer of metal, the second layer of insulation, and the last layer of metal. In the proposed structure, the base layer is a continuous plate and the second and third layers are alternate and ring-shaped. The cross-sections from the proposed structure are depicted in Fig. 1b. Also, for comparison of performance parameters, the disk-shaped biosensors are simulated. Figure 1c shows the layer arrangement of simulated disk biosensors. In each case, the first and third layers are from one type of metal. In this research, two types of metal, Au and Ag, are used, and SiO_2 is used as an insulation section. The Au refractive indexes are extracted from the Johnson and Christy [25] data, and the Ag and SiO_2 refractive indexes are extracted from Palik data [26].

The refractive index of PSA is presented in Table 1, which is calculated from the results of [27] using the following equation:

$$\Delta\lambda_{max} = S\Delta n \tag{1}$$

Here $\Delta\lambda$ represents the wavelength changes with increasing refractive index, S represents the sensitivity to refractive index, and Δn represents the refractive index changes. PSA samples ranging from 50 (1.7 ng/mL) to 600 pM (20.4 ng/mL) [27]. According to [28], a PSA concentration above 4 ng/ml is important for diagnosing prostate cancer, so we used four cases of 100, 200, 300, and 400 pM.

In our simulations, a plane wave light source is irradiated on a biosensor from the top side in different wavelengths. The perfectly matched layer (PML) boundary conditions are applied in the direction of light radiation and periodic boundary conditions in the direction perpendicular to the light radiation. The sensor's sensitivity for wavelength interrogation can be defined as [29].

$$s_\lambda = \frac{\Delta\lambda}{\Delta n_s} \tag{2}$$

Here d_λ is the differential change of the wavelength due to dn_sanddn_s is the refractive index change of the sensor layer. We define the figure of merit (FOM) of the sensor as Eq. (3) [30].

$$\mathrm{FOM} = \frac{\mathrm{S}_\lambda}{\mathrm{FWHM}} \tag{3}$$

where FWHM implies full width at half maximum.

Results and Discussions

In this section, we aim to select the optimal structures by analyzing the simulation results and comparing them. Due to the same path of determining the most optimal

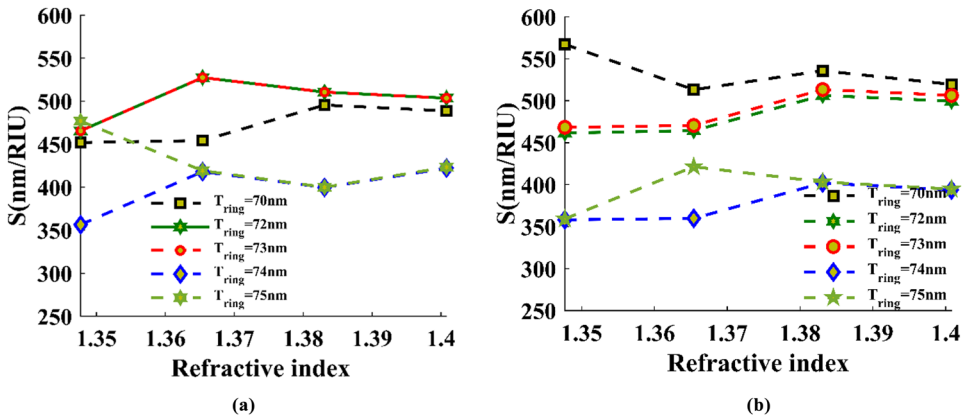

Fig. 4 Sensitivity as a function of refractive index **a** Au ring-shape nanoparticles and **b** Ag ring-shape nanoparticles

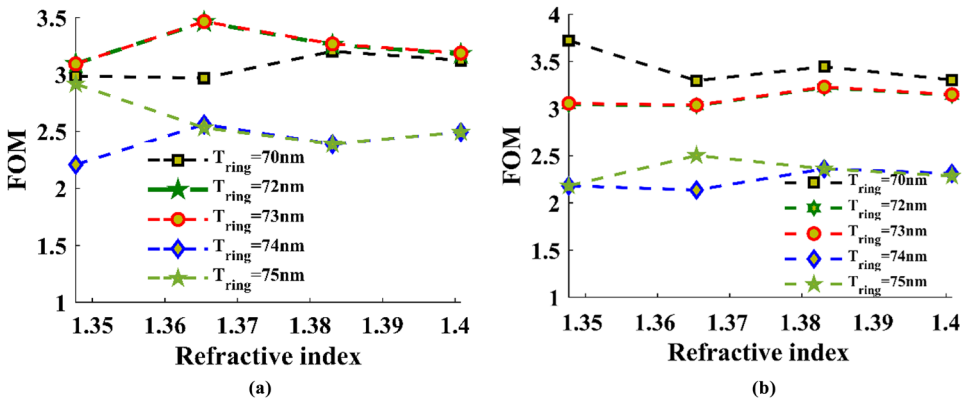

Fig. 5 FOM as a function of refractive index **a** Au ring-shape nanoparticles and **b** Ag ring-shape nanoparticles

dimensions of the ring biosensor and preventing duplication using the two metals Ag and Au, we only bring the Au steps in this section. In Fig. 2a, the effect of the inner radius of the ring (r_{in}) is simulated. According to the figure, the spectral response of the designed biosensors with radii of 55 and 50 nm are very similar, but we chose the spectral response of 55 nm because of their proximity to the telecommunication window. In Fig. 2b, the effect of the ring thickness (T_{ring}) on the reflection spectrum is calculated in terms of depth or maximum reflection and FWHM. The ring with a thickness of 72 nm is selected. In Fig. 2c, the effect of the distance of the rings from each other is compared, and the distance of 130 nm is selected due to high reflection and low FWHM.

In Fig. 3a, the effect of changing the height of the metal (h_{Au}) is presented; here, 30 nm is selected for the above-mentioned reason. Figure 3b shows the effect of SiO_2 insulation height (h_{SiO2}) changes that we choose 25 nm for the maximum depth and lower FWHM. According to the results, d and T_{ring} have the most negligible effect, and as mentioned in [31], the high effect of insulation thickness (h_{SiO2}), has the highest effect.

The biological substances can be measured using proposed structures through spectral changes. For biosensors, a high figure of merit and high sensitivity is more desirable. So, here both of them are calculated and compared. In Fig. 4a and b, we show the sensitivity of a proposed structure for different T_{ring} for Au and Ag, respectively. According to the diagram, the highest sensitivity of 567.2 nm/RIU is related to Ag with $T_{ring} = 70$ nm. The highest sensitivity of Au at $T_{ring} = 72$ nm and $T_{ring} = 73$ nm is approximately equal to 527.4 nm/RIU. In Fig. 5a and b, we have examined the FOM for different T_{ring} for Au and Ag, respectively. Here also, Ag has better performance, and the maximum FOM at $T_{ring} = 70$ nm is 3.72.

The sensitivity and FOM of the proposed structure by varying the environment refractive index depict that using an Ag ring has better performance. Here, the performance parameters of ring-shaped nanoarrays and disk shape one are compared. In Fig. 6a, we compare the reflection of ring-shaped and disk shape biosensors with Ag and Au nanoparticles, which shows the better performance of ring-shaped reflection. In Fig. 6b, we have compared the sensitivity with different shapes. This diagram clearly shows the superiority of the biosensor in the form of a ring, and also, the superiority of Ag over Au in both different shapes is visible.

Here, the excellent potential of the designed structure is used to examine them as a biosensor for the early diagnosis of prostate cancer. Identifying the amount of PSA can help us to be aware of prostate cancer. PSA is a protein produced by cancerous and noncancerous prostate tissue. Usually, a

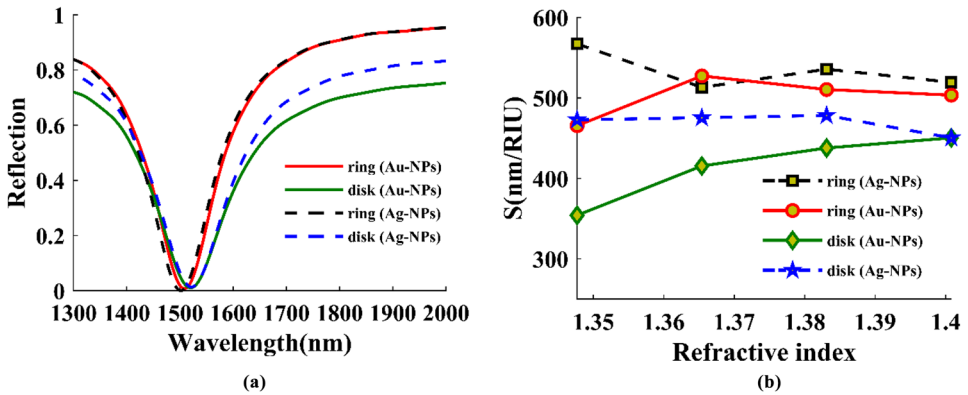

Fig. 6 **a** Comparison of the reflection of ring- and disk-shape Ag and Au NPs and **b** comparison of the sensitivity of ring and disk shape Ag and Au NPs

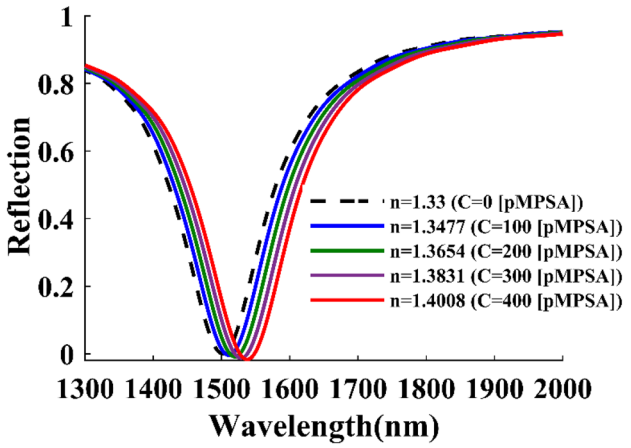

Fig. 7 Reflection as a function of wavelength for different refractive indices (concentration) where a redshift occurs

small amount of PSA enters the blood. Prostate cancer cells typically produce more pre-PSA than noncancerous cells, leading to higher levels of PSA in the blood. Our simulated results show that the ring shape based on MIM structure is a highly sensitive plasmonic biosensor in the communication window, and it is an appropriate candidate for PSA detection. The sensing strategy is based on the plasmonic effect and the shift of resonance peak due to refractive index changes of the surrounding medium of nanorings due to the existence of PSA. As mentioned, the refractive index is defined as $n = n_0 + \Delta n$. Here, all the data are calculated concerning the water state ($n_0 = 1.33$). With increasing the concentration of PSA, changes in the refractive index are accompanied by a red-shift of surface plasmon resonance (see Fig. 7).

In Table 2, we have provided the information of biosensors with two shapes of ring and disk with different metal nanoparticles, Au and Ag. Benefiting from the excellent refractive index sensitivity designed systems, our results show sensitivity higher than 500 nm/RIU, which is more sensitive than previously reported sensitivity [27]. It is important to mention that in [27], the sensitivity of 116 nm/RIU has been reported for Au nanodisks array-based biosensor for detecting PSA. Here, this value is increased to higher than 500 nm/RIU using MIM structures in the form of nanorings. Some prostate cancers may not produce large amounts of PSA, and higher sensitive biosensors are the more appropriate choice for detecting such PSA levels. However, the findings of this work reveal that it is possible to detect different PSA concentrations with higher sensitivity.

In the case of the fabrication process of our design biosensor, it is important to mention that such a structure can be fabricated using a combined protocol of electron beam lithography (EBL) and thermal evaporation [32–35]. Due to the use of silver nanoparticles (AgNPs) in our proposed structure, which are nontoxic, highly compatible with biomolecules, high catalytic activity, antibacterial activity towards microbes without the release of toxic biocides, and exceptional physical and chemical properties, that lead to the high stability of the biosensor [36, 37]. Also, our proposed structure has an absorbance near 100%, close to the information telecommunication window, as shown in Fig. 8. Because of such high absorption and tunability, this proposed configuration is highly recommended for many other optical applications like absorbers and imaging. The proposed plasmonic device can also be utilized in the hot electron-based plasmonic modulators and switches because of the narrow perfect absorption close to the information's communication window.

Table 2 The performance parameters of proposed structures in different PSA concentrations in water ($n_0 = 1.33$)

		C (PmPSA)	Δn	$\Delta\lambda$ (nm)	S (nm/RIU)	FWHM (nm)	FOM
Disk	Au	100	0.0177	6.27	354.23	160	2.21
		200	0.0354	14.71	415.53	161.79	2.56
		300	0.0531	23.25	437.85	165.53	2.64
		400	0.0708	31.89	450.42	167.39	2.69
	Ag	100	0.0177	8.37	472.88	162.34	2.91
		200	0.0354	16.83	475.42	163.7	2.90
		300	0.0531	25.4	478.34	165.53	2.89
		400	0.0708	31.89	450.42	171.76	2.62
Ring	Au	100	0.0177	8.24	465.53	150.53	3.09
		200	0.0354	18.67	527.4	152.19	3.46
		300	0.0531	27.11	510.5	156.2	3.26
		400	0.0708	35.65	503.5	157.95	3.18
	Ag	100	0.0177	10.04	567.23	152.35	3.72
		200	0.0354	18.17	513.17	155.68	3.29
		300	0.0531	28.45	535.78	155.52	3.44
		400	0.0708	36.78	519.49	157.24	3.30

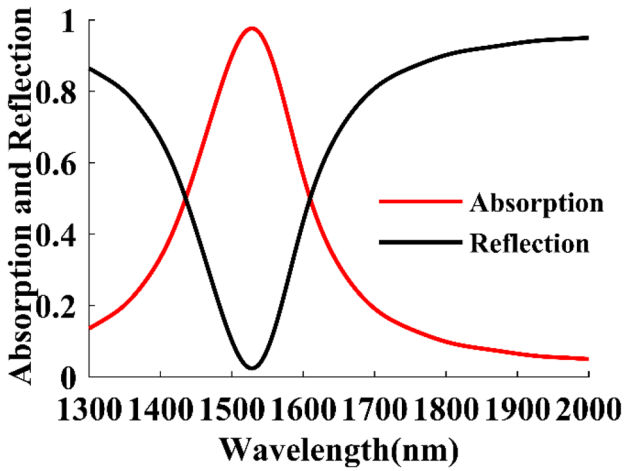

Fig. 8 Reflection and absorption of our designed structure as a function of wavelength

Conclusion

Due to the fatality of cancer and the need for early detection, in this study, we tried to achieve a biosensor with high sensitivity and a high figure of merit (FOM). According to our simulated results, we recommend a ring-shaped Ag nanoparticle biosensor to detect PSA with a sensitivity of 567.23 nm/RIU and FOM of 3.72 that can detect PSA well. Due to its less complexity, it is easy to build and can be used in real biosensors technologies. The proposal is analyzed using an FDTD method. According to the results, we can reach high-sensitivity and easy-to-fabricate sensors with the MIM topology. It is important to mention that the sensitivity of 116 nm/RIU has previously been reported for Au nanodisks arrays-based biosensors for detecting PSA. Here, this value is increased to higher than 500 nm/RIU using MIM structures in the form of nanoring. The findings of this work reveal that it is possible to detect different PSA concentrations with higher sensitivity.

Acknowledgements The author would like to express their sincere thanks to the University of Mohaghegh Ardabili for their technical support.

Data Availability The datasets analyzed during the current study are available from the corresponding author on reasonable request.

Materials Availability The datasets analyzed during the current study are available from the corresponding author on reasonable request.

Code Availability Not applicable.

Declarations

Ethics Approval Not applicable.

Consent to Participate Not applicable.

Consent for Publication Not applicable.

Conflict of Interest The authors declare no competing interests.

References

1. Siegel RL, Miller KD, Goding Sauer A, Fedewa SA, Butterly LF, Anderson JC, Cercek A, Smith RA (2020) Jemal A (2020) Colorectal cancer statistics. CA Cancer J Clin 70(3):145–164
2. Cabarkapa S, Perera M, McGrath S, Lawrentschuk N (2016) Prostate cancer screening with prostate-specific antigen: a guide to the guidelines. Prostate Int 4(4):125–129
3. Hugosson J, Roobol MJ, Månsson M, Tammela TL, Zappa M, Nelen V, Kwiatkowski M, Lujan M, Carlsson SV, Talala KM, Lilja H (2019) A 16-yr follow-up of the European randomized study of screening for prostate cancer. Eur Urol 76(1):43–51
4. Toner L, Papa N, Perera M, Katelaris N, Weerakoon M, Chin K, Harewood L, Bolton DM, Lawrentschuk N (2017) Multiparametric magnetic resonance imaging for prostate cancer–a comparative study including radical prostatectomy specimens. World J Urol 35(6):935–941
5. Ahmed HU, Bosaily AES, Brown LC, Gabe R, Kaplan R, Parmar MK, Collaco-Moraes Y, Ward K, Hindley RG, Freeman A, Kirkham AP (2017) Diagnostic accuracy of multi-parametric MRI and TRUS biopsy in prostate cancer (PROMIS): a paired validating confirmatory study. Lancet 389(10071):815–822
6. Kasivisvanathan V, Rannikko AS, Borghi M, Panebianco V, Mynderse LA, Vaarala MH, Briganti A, Budäus L, Hellawell G, Hindley RG, Roobol MJ (2018) MRI-targeted or standard biopsy for prostate-cancer diagnosis. N Engl J Med 378(19):1767–1777
7. Ito K, Yamamoto T, Ohi M, Kurokawa K, Suzuki K, Yamanaka H (2003) Free/total PSA ratio is a powerful predictor of future prostate cancer morbidity in men with initial PSA levels of 4.1 to 10.0 ng/mL. Urology 61(4):760–764
8. Loeb S, Catalona WJ (2014) The Prostate Health Index: a new test for the detection of prostate cancer. Ther Adv Urol 6(2):74–77
9. Lind K, Kubista M (2005) Development and evaluation of three real-time immuno-PCR assemblages for quantification of PSA. J Immunol Methods 304(1–2):107–116
10. Nam JM, Thaxton CS, Mirkin CA (2003) Nanoparticle-based bio-bar codes for the ultrasensitive detection of proteins. Science 301(5641):1884–1886
11. Grubisha DS, Lipert RJ, Park HY, Driskell J, Porter MD (2003) Femtomolar detection of prostate-specific antigen: an immunoassay based on surface-enhanced Raman scattering and immunogold labels. Anal Chem 75(21):5936–5943
12. Wee KW, Kang GY, Park J, Kang JY, Yoon DS, Park JH, Kim TS (2005) Novel electrical detection of label-free disease marker proteins using piezoresistive self-sensing micro-cantilevers. Biosens Bioelectron 20(10):1932–1938
13. Khani S, Danaie M, Rezaei P (2018) Realization of single-mode plasmonic bandpass filters using improved nanodisk resonators. Optics Commun 420:147–156
14. Khani S, Danaie M, Rezaei P (2019) Design of a single-mode plasmonic bandpass filter using a hexagonal resonator coupled to graded-stub waveguides. Plasmonics 14(1):53–62
15. Lee Y, Kim SJ, Park H, Lee B (2017) Metamaterials and metasurfaces for sensor applications. Sensors 17(8):1726
16. Livani AM, Kaatuzian H (2015) Design and simulation of an electrically pumped Schottky-junction-based plasmonic amplifier. Appl Opt 54(9):2164–2173

17. Livani AM, Kaatuzian H (2015) Analysis and simulation of nonlinearity and effects of spontaneous emission in Schottky–junction–based plasmonic amplifiers. Appl Opt 54(19):6103–6110
18. Danaie M, Kiani B (2018) Design of a label-free photonic crystal refractive index sensor for biomedical applications. Photonics Nanostructures Fundam Appl 31:89–98
19. Dinish US, Balasundaram G, Chang YT, Olivo M (2014) Sensitive multiplex detection of serological liver cancer biomarkers using SERS-active photonic crystal fiber probe. J Biophotonics 7(11–12):956–965
20. Farmani A (2019) Three-dimensional FDTD analysis of a nanostructured plasmonic sensor in the near-infrared range. JOSA B 36(2):401–407
21. Sharma AK (2013) Plasmonic biosensor for detection of hemoglobin concentration in human blood: design considerations. J Appl Phys 114(4):044701
22. Ebrahimy MN, Moghaddam AB, Andalib A, Naziri M, Ronagh N (2015) Nanoscale biosensor based on silicon photonic cavity for home healthcare diagnostic application. Int J Nanosci 14(05n06):1550026
23. Danaie M, Shahzadi A (2019) Design of a high-resolution metal–insulator–metal plasmonic refractive index sensor based on a ring-shaped Si resonator. Plasmonics 14(6):1453–1465
24. Maier SA (2007) Plasmonics: fundamentals and applications, vol 1. Springer, New York, p 245
25. Johnson PB, Christy RW (1972) Optical constants of the noble metals. Phys Rev B 6(12):4370
26. Palik ED (1998) Handbook of optical constants of solids, vol 3. Academic Press, US
27. Khan Y, Li A, Chang L, Li L, Guo L (2018) Gold nano disks arrays for localized surface plasmon resonance based detection of PSA cancer marker. Sens Actuators B Chem 255:1298–1307
28. Smith DS, Humphrey PA, Catalona WJ (1997) The early detection of prostate carcinoma with prostate specific antigen: the Washington University experience. Cancer Interdiscip Int J Am Cancer Soc 80(9):1852–1856
29. Homola J, Koudela I, Yee SS (1999) Surface plasmon resonance sensors based on diffraction gratings and prism couplers: sensitivity comparison. Sens Actuators B Chem 54(1–2):16–24
30. Shalabney A, Abdulhalim I (2012) Figure-of-merit enhancement of surface plasmon resonance sensors in the spectral interrogation. Opt Lett 37(7):1175–1177
31. Schaffernak G, Krug MK, Belitsch M, Gašparić M, Ditlbacher H, Hohenester U, Krenn JR, Hohenau A, (2018) Plasmonic dispersion relations and intensity enhancement of metal–insulator–metal nanodisks. ACS Photonics 5(12):4823–4827
32. Large N, Aizpurua J, Lin VK, Teo SL, Marty R, Tripathy S, Mlayah A (2011) Plasmonic properties of gold ring-disk nanoresonators: fine shape details matter. Opt Express 19(6):5587–5595
33. Tripathy S, Marty R, Lin VK, Teo SL, Ye E, Arbouet A, Saviot L, Girard C, Han MY, Mlayah A (2011) Acousto-plasmonic and surface-enhanced Raman scattering properties of coupled gold nanospheres/nanodisk trimers. Nano Lett 11(2):431–437
34. Teo SL, Lin VK, Marty R, Large N, Llado EA, Arbouet A, Girard C, Aizpurua J, Tripathy S, Mlayah A (2010) Gold nanoring trimers: a versatile structure for infrared sensing. Opt Express 18(21):22271–22282
35. Lin VK, Teo SL, Marty R, Arbouet A, Girard C, Alarcon-Llado E, Liu SH, Han MY, Tripathy S, Mlayah A (2010) Dual wavelength sensing based on interacting gold nanodisk trimers. Nanotechnology 21(30):305501
36. Elhakim HK, Azab SM, Fekry AM (2018) A novel simple biosensor containing silver nanoparticles/propolis (bee glue) for microRNA let-7a determination. Mater Sci Eng C 92:489–495
37. Raghavendra UP, Thipperudrappa J, Basanagouda M, Melavanki RM (2016) Influence of silver nanoparticles on spectroscopic properties of biologically active iodinated 4-aryloxymethyl coumarin dyes. J Lumin 172:139–146